PCCP

Accepted Manuscript

ROYAL SOCIETY OF CHEMISTRY

www.rsc.org/pccp

Cite this: DOI: 10.1039/c0xx00000x

www.rsc.org/xxxxxx

ARTICLE TYPE

Intramolecular charge transfer in aminobenzonitriles and tetrafluoro counterparts: fluorescence explained by competition between low lying excited states and radiationless deactivation. Part II: Influence of substitution on luminescence patterns

Mireia Segado, Yannick Mercier, Isabel Gómez, Mar Reguero*[a]

Received (in XXX, XXX) XthXXXXXXXXX 20XX, Accepted Xth XXXXXXXXX 20XX
DOI: 10.1039/b000000x

In this paper we study the mechanisms of charge transfer, luminescence and radiationless decay of three derivatives of 4-aminobenzonitrile (ABN): dimethyl-ABN (DMABN) and their tetrafluorinated derivatives, ABN-4F and DMABN-4F. Our CASSCF/CASPT2 computations explain the different luminescent patterns observed in these three compounds and in comparison with the parent system, ABN, in spite of their similar architecture. We have found that the modifications made by the different substitutions in ABN tune the relative energies of the locally excited (LE) and charge transfer (CT) excited states due to electronic and structural factors. In all cases the only potentially emitting species of CT character is the twisted-ICT. The increasing stabilization of this later species in the series formed by ABN-4F, DMABN and DMABN-4F explains the increasing intensity of the anomalous emission band in these compounds. Nevertheless, other factors like probability of emission v.s. nonradiative decay must also been taken into account. In fact fluoro-substitution increases the accessibility to conical intersections of the excited states with the ground state, opening an internal conversion channel that decreases the fluorescence quantum yield in the fluorinated derivatives. Our results also show that the involvement of the π–σ* state in the CT process is only possible in ABN-4F, but even in this case it is not probable.

Introduction

This paper is the second of a series of two papers devoted to the study of the photochemistry of the aminobenzonitrile (ABN) family of compounds. The parent compound ABN and the dimethyl derivative (DMABN) are the prototype of π-electron donor-acceptor compounds that, although being very similar, show very different luminescent patterns. While ABN shows only a normal fluorescence band, independently from the environment,[1] DMABN shows normal fluorescence in gas phase but dual fluorescence in polar solvents.[2] It is unanimously accepted that the normal band corresponds to emission from a locally excited (LE) state, while the anomalous band is generated by emission from an intramolecular charge transfer (ICT) excited state.[3] Much effort has been devoted to determine the species responsible of the anomalous emission and elucidate the mechanism of charge transfer, from the experimental as well as from the theoretical points of view (see the review of reference 3), but these questions are still a subject of debate.

Some authors of this paper studied some time ago the photochemistry of ABN and DMABN from the theoretical point of view, and explained the general features of the CT mechanism and the origin of the normal and anomalous fluorescence bands. [4] Later publication of new hypothesis about the CT mechanism,[5] though, made us consider convenient a revision of this subject.

For doing so, we first revisited the photochemistry of ABN, using a more accurate computational methodology to develop the new study and exploring novel possible reaction paths (results published in Part I of this series of two papers, reference 6). To provide more data that could help to understand and rationalize the phenomena studied, we decided to tackle also the study of some ABN derivatives that, in spite of their similar architecture, show different luminescent characteristics from ABN. They are 1,2,3,4-tetrafluoroaminobenzonitrile (ABN-4F), and 1,2,3,4-tetrafluorodimethyl-ABN (DMABN-4F) (Scheme 1), which results are presented in this paper. We also include here results for DMABN, recomputed at the same level of calculation, for comparative purposes. We expected that the results for the different systems showed qualitative changes when compared with ABN so that they shed light in the mechanisms of the photochemical processes that these compounds undergo. Additionally, if the luminescence predicted by our results for these derivatives agreed with the experimental observations, we would have a strong support for our hypothesis of the mechanism of the charge transfer process in aminobenzonitriles.

Thanks to the information obtained for ABN in our previous work, in the study of its derivatives we will address mainly the

states involved in the charge transfer reaction and the areas of the potential energy surfaces (PES) crucial to explain the photophysics of these systems.

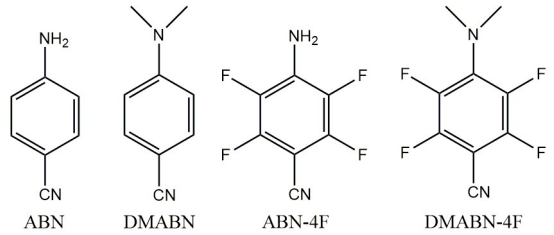

Scheme 1

Regarding the first point, the low-lying states that can be involved in the charge transfer process are the following.

The LE state is a locally excited state, resulting from a $\pi \rightarrow \pi^*$ excitation of orbitals located on the ring.

There are two ICT states generated by the excitation of an electron from the lone pair of the amino nitrogen to a quinoid or antiquinoid antibonding orbital of the ring that are named, consequently, ICT(Q) and ICT(AQ) respectively. Relaxation on these states lead to high energy minima where aminobezonitriles show a planar geometry giving place to the planar ICT (PICT) species, or to low energy minima where the amino group is twisted, giving place to the twisted TICT(Q) and TICT(AQ) species.

The ICT(CN) state results from an excitation of an electron from the lone pair of the amino nitrogen to an antibonding π orbital of the cyano group. This causes a rehybridation of the C atom from sp^3 to sp^2. The species that results from relaxation on this surface shows the cyano group bending, and is named rehybridized ICT, RICT.

The areas of the PES of interest to explain the photophysics of the systems studied are those of the minima that can be populated and the paths that connect them. But the radiationless deexcitation channels must also be explored. With this information the most probable processes for each system must be determined, on the bases of thermodynamic and kinetic factors.

In ABN, only the species LE, TICT(Q) and RICT correspond to minima located on the lowest excited state potential energy surface S_1. When ABN is irradiated, the excitation populates the S_2-ICT(Q) state. The relaxation on this surface leads first to the population of the PICT minimum located on the S_2 PES. But near this geometry there is a $S_2(ICT)/S_1(LE)$ conical intersection that can be reached along a barrierless path from the PICT minimum. The LE state will be then fast and efficiently populated through this CI. But apart from crossing to the LE surface, the system can continue in the ICT(Q) state. In this case, further relaxation will lead to the TICT(Q) minimum, located on the S_1 surface but higher in energy that the LE one. Another possible, although less probable path, is the crossing to the ICT(CN) surface. This process would take place through a $S_3(ICT(CN))/S_2(ICT(Q))$ conical intersection located slightly higher in energy than the initial excitation. Relaxation along the ICT(CN) surface will lead to the population of the RICT minimum, also located on the S_1 surface, but higher in energy than the LE and TICT ones. Given that all these minima are interconnected through low energy paths and that the LE is favoured thermodynamically and kinetically, TICT and RICT are quickly depopulated in favour of the LE species. This landscape explains why ABN only shows normal fluorescence.

Radiationless deactivation pathways for ABN were also searched for. We found several $S_1(LE)/S_0$ and $S_1(CT)/S_0$ conical intersections at geometries where different C atoms of the phenyl ring were puckered. The barriers to reach these crossing points are moderate, such that they can be overcome with the contribution of thermal energy. It means that at high temperature there is an internal conversion channel accessible, what constitutes a path for radiationless deactivation. This fact explains the decrease of fluorescence quantum yield observed experimentally when the temperature increases.

In general the results obtained for ABN explain the experimental observations, and the computational quantitative data agree satisfactorily with the experimental measurements. This gives us a sound basis to focus the study of the ABN derivatives on the same species and processes (or in other words, on the same minima and paths) that were found to determine the photochemistry of the parent system.

The work reported in this paper shows that for the systems studied here there are four possible luminescent species: LE, TICT(Q), TICT(AQ) and RICT. The actual emission from one or another depends not only on thermodynamic factors, i. e. relative energies, but also on dynamic factors (analysed individually and in comparison for ABN, ABN-4F, DMABN and DMABN-4F) given by the competition between alternative paths like emission (which probability is calculated theoretically by the oscillation strength parameter) or radiationless deactivation (through an internal conversion between the S_1 excited state and the ground state). Only considering all these factors the luminescent behaviour of the systems studied can be explained satisfactorily.

The allocation of excited-states structures and the clarification of the mechanisms of the reactions of these systems will be successfully attained by the use of the ab initio CASSCF/CASPT2 methodology. The good agreement of our theoretical results with the experimental findings will support the mechanisms proposed in this work.

Derivatives studied

The ABN derivatives of this study have been chosen taking into account that there are two ways of modifying the parent system to get significant changes on the ICT reaction: a) modifying the structure of the amino moiety and b) modifying the benzonitrile moiety.

Concerning the modification of amino moiety, most of the 4-aminobenzonitriles with a tertiary amino group undergo ICT reaction, but this generally does not occur for molecules that have a secondary amino substituent.[1] Furthermore, ICT has never been reported for aminobenzonitriles with a primary group such as ABN. Also, compounds where the amino group is enforced to be twisted show only the CT fluorescence band supporting the TICT hypothesis,[2,4] but other rigid derivatives that can twist only partially and still show the anomalous band, suggest that the PICT structure is the emitting species.[7] However, it has been shown that some bicyclic systems like 1-*tert*-butyl-6-cyano-

1,2,3,4-tetrahydroquinoline and 1-methyl-7-cyano-2,3,4,5-tetrahydro-1H-1-benzazepine, are flexible enough to be able to twist and adopt a stable TICT structure capable of emitting.[8]

Concerning the modification in the benzonitrile moiety, the charge transfer process can be enhanced enlarging the acceptor character of this part of the molecule by adding additional acceptor substituents. The addition of more cyano groups to bezonitrile has a mesomeric effect, but it leads to a modification of the S_1 and S_2 surfaces.[9] These possible changes can be avoided by the introduction of substituents with a predominantly inductive influence, leaving the nature of S_1 and S_2 surfaces largely intact. This could be achieved, for example, by fluoro substituents. It has been shown by comparison of the reduction potentials of benzonitrile and fluorobenzenes[10] that it is necessary up to six F atoms to increase the electron acceptor character as much as a with a single nitrile group. The small electron affinity of F makes it possible to enlarge the acceptor character of the benzene moiety step by step,[11] leading to a more controlled process.

Thus, Zachariasse et al. investigated the introduction of a fluoride atom into different positions of the benzene ring in 4-aminobenzonitrile derivatives, and stated that there is no indication of ICT emission in alkane solvents, but the internal conversion (IC) responsible of the radiationless deactivation is enhanced by the fluoro substituent.[12] Neither the introduction of two F-substituents in the phenyl ring of ABN (in the 2,5-difluoro-4-aminobenzonitrile) are sufficient to induce an ICT reaction.[13] However, for the tetrafluoro-aminobenzonitrile derivatives, unlike ABN and DMABN, the fluorescence spectra, both in polar and non polar solvents, consist only of ICT emission while the fluorescence band from the LE cannot be detected.[12,13,14] It evidences the easier population of the CT excited state in these derivatives as compared to their non fluorinated counterparts. It means that fluoro substituents can decrease the energy gap $\Delta E(S_1,S_2)$, making the 2,3,5,6-tetrafluoro-4-ABN the first donor-acceptor molecule with a primary amino group for which ICT emission is observed.[13]

Regarding other competitive photochemical reaction paths, Zachariasse and co-workers observed that the fluorescence decay time and quantum yield strongly decrease with increasing the temperature in DMABN and ABN in alkane solvents.[12] They have established that DMABN and ABN undergo efficient thermally activated IC. Thus, IC becomes the dominant deactivation pathway of the first excited singlet state S_1 at high temperatures. The number of fluorine substituents seems to be also an important factor in the opening of this IC channel, enhancing the accessibility to a conical intersection that leads back to the electronic ground state. The internal conversion yield in n-hexane at 25ºC is considerable larger for ABN-4F (~1.00) and for 2,3,5,6-tetrafluoro-4-aminobenzonitrile (DMABN-4F) (0.92) than for ABN (0.10) and DMABN (0.10). Thus, in the tetrafluorinated aminobenzonitriles, both the IC channel and the induced ICT emission are enhanced as compared with non substituted ones.[12,13,15]

Computational details

The computational methodology used in this work is the same than the one used in the previous study for ABN (part I of this series of papers): the CASSCF/MS-CASPT2 strategy. The active space used in general includes 12 electrons and 11 orbitals: the benzene π and π* orbitals, the amino nitrogen lone pair, and the four π and π* orbitals of the cyano group (See Figure S1 of ESI†). But in ABN-4F, in order to take into account the possible involvement of $\pi-\sigma^*_{C\text{-}F}$ states, a bigger active space was used for some test calculations. We added to the previous active space an additional $\sigma^*_{C\text{-}F}$ orbital that comprises the totally symmetric combination of antibonding C-F σ* orbitals.

The basis set used here for the geometry optimizations was a 6-31G* one[16] instead the cc-pVDZ. This decision was made after comparing the geometries obtained in previous works for ABN with both basis sets[6]: the changes in the geometries were not significant, so for the derivatives studied here the 6-31G* basis set was used for all geometry optimizations, which were performed without any symmetry constrain.

To incorporate the effect of the dynamic valence electron correlation, MS-CASPT2/cc-pVDZ single point energies of the critical points were calculated at the CASSCF geometries, but energy paths were calculated at the MS-CASPT2/6-31G* level instead. Conical intersections were optimized at the CASSCF level, so the MS-CASPT2 energies of the minimum energy points of the conical intersections reported in the text and tables will be the average of the energies of the states involved in the corresponding CI.

Exceptions to these general lines made in some specific cases are commented explicitly along the text when happening.

Numerical frequency calculations were run to determine the nature of the stationary points.

The transition dipole moments and oscillator strengths were computed with the CAS state interaction (CASSI) protocol[17] using Perturbed Modified (PM) CAS-CI wavefunctions.

To obtain profiles of the PES, minimum energy paths (MEP) at CASSCF level or linearly interpolated internal reaction coordinate (LIIRC) paths between critical points at CASPT2 level, were calculated in areas of interest. The LIIRC paths are built modifying simultaneously all the internal coordinates of the system to change step by step the geometry of the initial point of the path to obtain the geometry of the last point. The highest point of the profile of this path gives an upper limit for the barrier of the reaction path that joins both structures.

Valence-Bond structures were determined for DMABN-4F using the results of the computation of the second order exchange density matrix and the diagonal elements of the electronic density matrix (See Figure S2 of ESI†). The elements P_{ij} have a simple physical interpretation, which is related to the spin coupling between the electrons localized in the orbitals residing on the atoms i and j. An illustration of the meaning of these matrix elements can be found in reference 18. Analogous results for ABN and DMABN can be found in ref 4.

We used the Gaussian 09[19] and MOLCAS 7.0[20] program packages.

Results and discussion

This section is structured in five subsections. In the first one, we collect the results of the calculation of the initial photoexcitations,

which are related to the absorption spectra. In the second section, we show the stable structures found on the PES of the different excited states involved in the process. In the next two subsections we characterize paths between different critical points of the PES studied. The information of these four subsections forms a global picture that allows us to suggest in the fifth subsection the mechanisms of the photophysical and photochemical processes that explain the luminescence observed in the systems studied. We will also mention the previous results for ABN6 (reported in more detail in Part I) and DMABN (reported in ref. 4 and recalculated here) for comparison purposes.

Ground state geometry and absorption spectrum.

The optimized ground-state (S_0–GS) structures obtained are shown in Figure 1. The ground-state geometries of ABN, DMABN and ABN-4F are untwisted with a pyramidal amino group with wagging angles of 25.7º, 43.0º and 40.0º respectively, slightly larger than experimental values of 11.9º and 15º in DMABN[21,22] and 35º in ABN.[22]

Fig 1 Geometry of the ground state minima of ABN, ABN-4F, DMABN and DMABN-4F optimized at CASSCF level. Bond distances in Å.

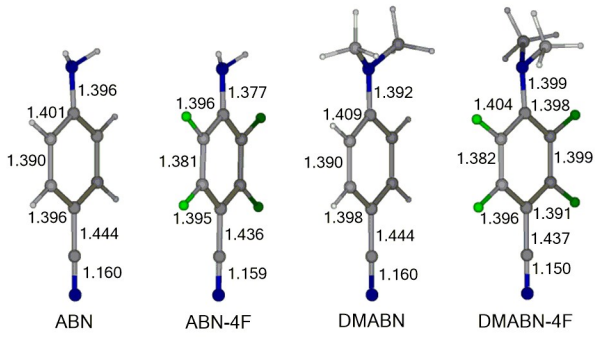

Because of the strong steric hindrance between the two methyl substituents of the amino group and the fluorine atoms in the benzene ring, the S_0-GS DMABN-4F structure has a twist angle of 55º, very different from the planar geometry of non-fluorinated systems. This angle is slightly larger than the 33º obtained from the X-ray data.[23] However, previous theoretical results predict twist angles ranged from 30º to 54º depending on the computational method employed.[24]

The experimental value of the dipole moment in non polar solvents for ABN-4F, 6.18D,[25] is also in good agreement with the computed value, 6.09D, like in the case of ABN (calculated value of 6.77D v.s. experimental value of 6.60D[26]) and DMABN (6.1D calculated value v.s. the value of 6.0D assumed in ref. 25). DMABN-4F shows the smallest dipole moment on the ground state (5.1D). As a whole, we observe that fluoro substitution increases the pyramidalization (in ABN-4F) or the twist angle (in DMABN-4F) of the amino group due to sterical repulsions. It is interesting to point out that DMABN-4F is the only of the molecules studied here with a sizable quantum yield of ICT fluorescence in hexane (0.0026),[13] what can be related with the twisted structure of its GS geometry.

Table **1** shows the computed CASPT2 results for vertical transitions at the Franck Condon (FC) geometry in gas phase, which can be compared with the energies of the maximum of the band of the experimental absorption spectra, also included in the table. The experimental data were obtained in nonpolar solvents.

Table 1. MS-CASPT2 vertical energies relative to the ground state minimum (in kcal mol^{-1}), dipole moments (in Debye), oscillator strengths (f) and experimental absorption energies in n-hexane[13] for the lowest energy states of ABN, DMABN, ABN-4F and DMABN-4F.

	State	E	μ	f	exp*
ABN	S_0	0	6.77		
	LE	106.25	6.30	0.004	
	ICT	121.21	9.76	0.450	109.4
DMABN	S_0	0	6.19		
	LE	93.3	6.01	0.006	92.2
	ICT	102.7	13.80	0.608	101.9
ABN-4F	S_0	0	6.09		
	LE	113.14	5.10	0.001	
	ICT	126.23	10.54	0.569	111.5
DMABN-4F	S_0	0	4.88		
	LE	97.9	5.03	0.009	
	ICT	95.7	14.22	0.318	95.5

The energy gap between the two excited states, $\Delta E(S_1\text{-}S_2)$, decreases as the substitution increases: it is 16.93 kcal·mol^{-1} for ABN, 13.09 kcal·mol^{-1} for ABN-4F, 8.24 kcal·mol^{-1} for DMABN and -6.25 kcal·mol^{-1} for DMABN-4F. The inversion of the LE and ICT states in the last case is in strong agreement with the fact that the weak shoulder ascribed to absorption to the LE (L_b-like) state in DMABN spectra is not visible in the spectrum of DMABN-4F in n-hexane.[14] This inversion of states will be enhanced in a polar solvent, which will stabilize the CT state even further.

Excited states stable structures

The emission properties of the systems depend on the population of the excited states minima, the probability of emission (related to f) and the competing radiationless deactivation pathways to S_0. We located on the S_1 PES minima corresponding to the LE, ICT(Q) and ICT(CN) structures (LE, TICT(Q) and RICT). The geometries are shown schematically in Scheme 2, and the geometrical parameters can be found in Figure S3 of ESI†, together with those of ABN and DMABN for comparative purposes. Energetics is collected in Table 2. To make easier the comparison of the excited states species, these energies are given relative to the energy of the LE minimum of each system. Energies of ABN are also included for comparison. Energies of DMABN have been recalculated at the MS-CASPT2/cc-pVDZ level at the geometries reported in ref. 4.

The S_1-LE structure has an anti-Kekulé benzene moiety in all cases. For ABN, DMABN and ABN-4F the hydrogen atoms of the amino group are slightly out of the plane, like in the ground state structure. The most important feature in ABN-4F is that the fluorine atoms (given their tendency of originating non planar structures) lye almost 23º out of plane of the benzene ring. DMABN-4F shows a LE twisted structure with a torsional angle of 88º. The C atom of the ring bonded to the amino group is pyramidalized, so this group is slightly out of the plane, like in the ground state structure. Some fluoro substituted compounds

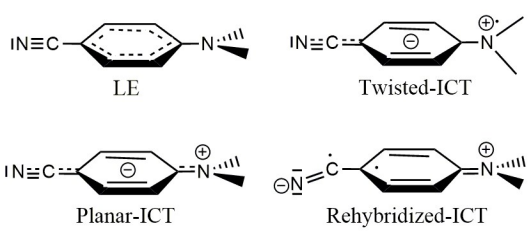

Scheme 2

show low energy excited states characterized by excitations from π molecular orbitals to $\sigma^*_{C\text{-}F}$. In order to check the involvement of these $\pi-\sigma^*_{C\text{-}F}$ states in this minimum and its effect on the out of plane distortion, a tests calculation was performed. A more extended active space was defined, (12 electrons in 12 orbitals) including the totally symmetric combination of C-F σ^* orbitals. The lowest energy excited state of ABN-4F was recalculated at the LE geometry. The analysis of its wavefunction confirmed that the $\pi-\sigma^*_{C\text{-}F}$ excitation is not involved in the description of this state and the LE minimum has a pure LE character.

Table 2. MS-CASPT2 adiabatic energies relative to the LE state minimum (in kcal mol^{-1}), of the optimized minima of the lowest energy excited states of ABN, DMABN, ABN-4F and DMABN-4F. Dipole moments (in D) in italics.

Min	S_1-LE	S_2-PICT	S_1-RICT	S_1-TICT(Q)	S_2-TICT(AQ)
ABN	0	14.59	19.74	10.54	33.60
	5.1	*11.2*	*10.5*	*10.8*	*13.8*
DMABN	0	8.44	22.81	0.10	14.60
	6.1	*13.8*	*16.8*	*13.5*	*14.1*
ABN-4F	0	Not found	19.14	4.58	46.70[a]
	5.3		*9.2*	*10.5*	*13.6*
DMABN-4F	0	Not found	22.90	-17.12	15.74
	4.8		*16.0*	*13.1*	*14.4*

a) Minimum located of S_3

S_1-TICT(Q) has a charge transfer character that gives rise to a large dipole moment. Regarding geometrical parameters, all the systems have a quinoidal distribution in the benzene ring and the amino group is pyramidalized as well as twisted, with N-phenyl bond lengths enlarged by 0.06Å (DMABN), 0.07Å (ABN), 0.05Å (DMABN-4F) and 0.09Å (ABN-4F) compared with the ground state. The computed dipole moments of S_1-TICT of ABN-4F and DMABN-4F (10.5D and 13.1D respectively) are in good agreement with the corresponding values of (13.6 ± 0.6)D and (13.8 ± 0.4)D estimated by Zachariasse for the ICT emitting species.[13] In the TICT(Q) geometry the PM-CAS-CI wavefunction is a mixture of a ICT(Q) and LE CASSCF functions, with almost equal weights. This characteristic was also found for ABN, but in the present case, enlarging the active space to a (14, 13) one, including the σ and σ^* orbitals of the bond between the ring and the amino group, the states were completely decoupled. This enlargement of active space did not change appreciably the energy obtained, so the (12, 11) active space was used for the rest of computations.

TICT(AQ) minima were found for all ABN derivatives, but these minima were located on the S_2 or S_3 PES, high above the quinoid structures: 14.50, 42.12 and 32.86 kcal·mol^{-1} for DMABN (on S_2), ABN-4F (on S_3) and DMABN-4F (on S_2) respectively. Therefore, the involvement of this species in the processes studied can be discarded and this state has not been investigated any longer.

The minima of the ICT(CN) state, which correspond to the RICT species, were found for all systems on the S_1 PES with similar characteristics: these structures show large dipole moments (consequence of its CT character), the rings have quinoid conformation, the bend angle is quite similar (121.1º, 121.6º, 123.8º and 123.0º for ABN, DMABN, ABN-4F and DMABN-4F respectively), and in all cases the energy is much higher than that of the corresponding LE and ICT(Q) species (See table 2). Consequently, although the ICT(CN) state could be involved in the mechanism of population of the bright ICT state, this minimum is definitely discarded as the luminescent species.

PICT structure was found on the S_2 surface for ABN and DMABN near FC region, but this minimum has not been located for tetrafluorinated counterparts. The reason of its absence of this ICT structure in these systems could be the strong steric hindrance between the fluorine atoms of the phenyl ring and the amino group.

Concerning the partially twisted ICT species (pTICT) lately proposed as the emitting species for DMABN,[27] we performed an exhaustive search in this system considering the possible effect of the size (and composition) of the active space, the size and type of the basis set and different geometrical constrains, but this minimum could not be located. Given that the location of the pTICT in ref. 27 was performed under a C_2 symmetry that allow the twist but not the pyramidalization of the C atom bonded to the amino group, the location of this minimum could well be an artefact of the optimization constrains, hidden by the impossibility of obtaining the frequencies in this type of calculation (performed with the MOLCAS package) that would have shown the character of the critical point located (perhaps a TS along the pyramidalization coordinate). Nevertheless, the PES of the ICT state is quite flat in the neighbourhood of the TICT minimum along the torsion coordinate, as shown in a previous computational work[28] for DMABN in polar solvents. This topology could explain the location of a spurious minimum that would be in any case very shallow and higher in energy that the TICT one.

Mechanisms of population of the S_1 minima

The oscillator strength values obtained in this study for the transitions to the excited states from the ground state at the FC geometry (see Table 1) indicate that, like in ABN, in all derivatives the state populated by the initial excitation is the ICT(Q) state.

For ABN we investigated three possible paths of decay from the S_2-ICT(Q) PES to the S_1 one: the ICT(Q)→LE path; the ICT(CN) mediated path and the ICT(Q)→ICT(AQ) path. We found that in ABN the probability of the last one was very low, given that the ICT(AQ) state was higher in energy than the ICT(Q) state at the FC area and even at the TICT(AQ) minimum. The same energetic characteristics are found for the ICT(AQ) states of ABN derivatives, so also in these cases this path can be discarded.

The ICT(CN) mediated path will be more probable for those systems where this state can cross with the ICT(Q) at low energies. A first hint of the accessibility of this crossing can be got from the energy difference between the TICT(Q) and RICT species. From the data in Table 2 we can see that this energy difference is 5.5, 14.5, 22.7 and 40.0 kcal·mol^{-1} for ABN, ABN-4F, DMABN and DMABN-4F. The probability of accessibility to the ICT(Q)/ICT(CN) crossing seems to be quite low for DMABN and DMABN-4F and even for ABN-4F, but we investigated this path in the last case to confirm our hypothesis.

At the FC geometry the ICT(CN) state was the seventh excited state in ABN-4F, 181.12 kcal·mol^{-1} above the ground state (CASSCF/CASPT2(12,11) level of calculation, with 13 states averaged). The relaxation along this surface stabilizes this state very fast, crossing the ICT(Q) state only 7.92 kcal·mol^{-1} above the initial excitation energy. The geometry of this S_3/S_2 ICT(Q)/ICT(CN) conical intersection shows a cyano group bent by 142.2º (Figure S4 of ESI†). Hence, depending on the vibrational excess energy in bending coordinates following photoexcitation, this CI can be accessed and the RICT minimum populated. Nevertheless, this is not the most probable path to populate the S_1 surface, as will be shown next.

To investigate the ICT(Q)→LE path we analysed the most probable relaxation paths on the ICT(Q) PES from the FC geometry (i.e., the first photochemical event after excitation). Our results reported in part I showed that ABN relaxes towards the PICT minimum, and from there the system reaches easily the S_2/S_1 ICT(Q)-LE conical intersection (as shown in a recent work of our group,[29] this CI also exists for planar geometries very near the FC geometry, so this internal conversion can be very fast). The same path was reported for DMABN in our previous work on this system.[4] In the work presented here, for DMABN we have only recalculated the energy of the critical points of this path at the same level of calculation than the results for the other systems to make possible the comparison. For the fluorinated derivatives, the energetics of ABN-4F and DMABN-4F show important differences that determine their different photophysical properties.

In the ABN-4F derivative, where there is not a stable PICT structure, the relaxation from FC (determined by a MEP calculation), leads directly to the S_2/S_1 ICT(Q)-LE conical intersection shown in Figure 2. Its branching space does not involve either the amino group twist or the pyramidalization coordinates, so the S_2/S_1 degeneracy will be preserved along the amino group torsion. Thus, $S_2 \rightarrow S_1$ internal conversion can take place over the full range of torsion angles, and both the S_1-LE and the S_1-TICT minima could be populated after internal conversion from any point of the seam.

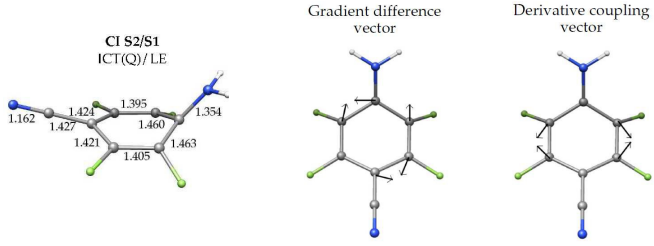

Fig. 2 Geometry of the ICT(Q)/LE (S_2/S_1) conical intersection and vectors of the branching space for ABN-4F.

The minimum energy point of this CI is placed 12.44 kcal·mol^{-1} below the excitation energy. The path linking adiabatically the LE and TICT minima shows, in Figure 3 (LIIC in Figure S5 of ESI†), that the barrier of the LE→TICT process is 5.7 kcal·mol^{-1} high, while the barrier of the backward process is only 0.3 kcal·mol^{-1}. It indicates that after the initial excitation both the LE and the TICT minima can be populated, but the thermodynamic equilibrium will favour the LE species.

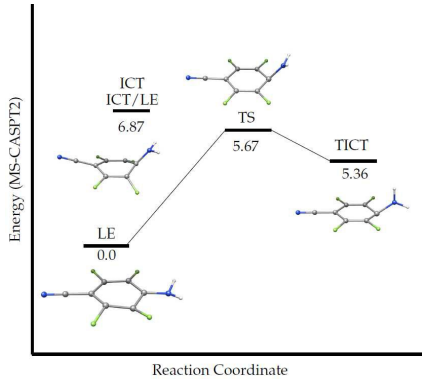

Fig. 3 Schematic potential energy profile of the adiabatic path and relative location of the CI connecting the LE and TICT minima for ABN-4F. Energies in kcal·mol^{-1}.

In the case of DMABN-4F, where the ICT(Q) state is the first excited state at FC, after the initial excitation the system tends to relax towards the TICT(Q) minimum in a barrierless process, as shown in Figure 4a. These results are consistent with the experimental observation of ultrafast formation of an emitting ICT species in DMABN-4F in contrast with DMABN.[13,14]

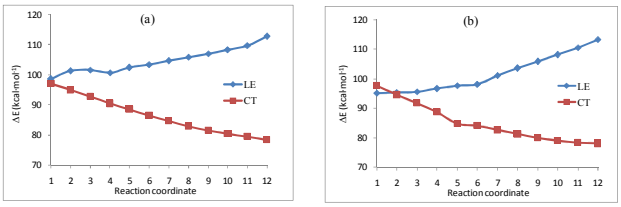

Fig. 4 MS-CASPT2 energy profiles of the LE and ICT states of DMABN-4F along LIIC path (a) from FC to TICT(Q) minimum; (b) from LE to TICT(Q) minimum. Energies in kcal·mol^{-1}.

Nevertheless, given that the LE minimum is located on S_1, the PES of the LE and ICT states must cross. The minimum energy point of this conical intersection (ICT(Q)/LE (S_2/S_1)) is very similar (in geometry as well as in branching space, Figure S6) to that found for ABN-4F, and lies only 0.6 kcal·mol^{-1}above the S_1-LE minimum. No transition state connecting adiabatically the LE and TICT minima could be located because of the flatness of the surface, so a linearly interpolated path was calculated between both minima (Figure 4b). It shows that the adiabatic barrier for the LE→TICT process is only 0.3 kcal·mol^{-1}, whereas the barrier for the backward process is 17.4 kcal·mol^{-1}high. Therefore, although both minima could be populated, in this case the equilibrium is strongly displaced towards the S_1-TICT species, explaining the presence of the ICT emission for DMABN-4F even in nonpolar solvents.

From these results we can conclude that for ABN-4F, the most

probable path of population of S_1 is through a crossing between the ICT(Q) and LE surfaces, although the mediated ICT(CN) path is also possible. On the other hand, for DMABN-4F, the population of the S_1-TICT(Q) minimum is direct, and the probability of population of the S_1-LE one is very low.

Nevertheless, to complete the landscape of the possible reactivity of these systems we still have to analyse the possibility of a radiationless deactivation path by internal conversion through a S_1/S_0 conical intersection.

Radiationless deactivation paths

It has been observed experimentally that F-substitution in the phenyl ring of aminobenzontriles leads to smaller fluorescence quantum yields and shorter decay times than in the parent compounds. The number of fluorine substituents seems to be an important factor in the opening of the internal conversion channel, enhancing the accessibility to a conical intersection that leads to the electronic ground state.

We will present here the results of the study of this channel for ABN-4F and compare them with the analogues ones obtained previously for ABN. In our previous work on DMABN, we had not studied this deactivation path, so to be able to compare between this system and its fluorinated counterpart, we have performed these calculations and now present here these results compared with those for DMABN-4F.

For ABN-4F, we found several crossing between S_1 and S_0 surfaces which geometries are shown in detail in Figure S8 of ESI†. All the CI structures correspond to different bends of the phenyl ring and puckering of different C atoms out of the ring plane. These geometries are similar to the ones obtained for ABN in our previous work.[6] We summarize schematically the different deactivation channels for ABN-4F in Figure 5 and collect the energetics in Table 3. It is worth remembering here that the geometry optimization of these critical points is only carried out at the CASSCF level, while the energetic is recalculated at the CASPT2 level. For this reason there can appear some inconsistencies between numerical values, given to the displacement of the critical points at different levels of calculation. Discrepancies are especially evident in the paths and CIs presented in this section, therefore to make the results more comprehensive, we also include in the tables CASSCF results. Nevertheless, comparisons of the CASPT2 energies between parent systems and fluorinated derivatives lead to the same qualitative conclusions than CASSCF results.

All the S_1/S_0 crossings are of LE/S_0 character except CI-4 that is ICT(Q)/S_0. In order to obtain the activation barriers, transition states of the paths from the LE minimum to the conical intersections were looked for. Only TS for the paths to CI-1 and CI-4 were found. The energies of the intersections and the transition states collected in Table 3 show that being the geometries of these critical points optimized at CASSCF/6-31G* level, it is difficult to establish accurately the height of the barriers of these processes at the CASPT2 level.

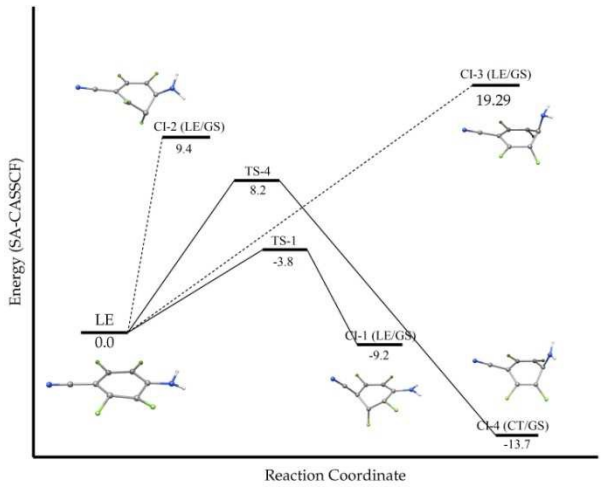

Fig. 5 Schematic profiles of the possible radiationless deactivation mechanism from S_1 for ABN-4F. Geometries optimized at CASSCF level, energies (in kcal mol^{-1}) obtained at MS-CASPT2 level.

Table 3. CASSCF and MS-CASPT2 energies relative to the LE minimum (in kcal·mol^{-1}) and dipole moments (in Debye) of the conical intersections and transition state (optimized at CASSCF level) involved in the radiationless deactivation of ABN-4F.

Structure	State	E (CASSCF)	μ	E (CASPT2)
CI-1	LE	2.4	7.45	-19.1
	S_0	3.3	4.44	0.7
CI-2	LE	18.1	6.43	4.2
	S_0	18.7	4.99	14.5
CI-3	LE	18.2	4.76	16.8
	S_0	18.3	5.04	20.2
CI-4	ICT	-2.3	10.88	-18.6
	S_0	-0.6	4.06	-8.8
TS-1	LE	3.5	6.82	-3.8
TS-4	ICT	11.9	5.53	8.2

To get a better estimate of some of these barriers, we calculated the profiles of the S_0 and S_1 surfaces along the path from the LE minimum to the CI-1, CI-2 and CI-3 at the SA2-CASSCF/CASPT2/6-31G* level (Figure S9 of ESI†). The lowest barrier was found along the way to CI-1, where the S_1 surface is so flat, that the activation barrier for this internal conversion channel is only about 3.0 kcal·mol^{-1}. Consequently we can consider this process barrierless, especially if we take into account the large amount of energy that the system retains from the initial excitation to the S_2 state. This result agrees satisfactory with the 3.0 and 4.6 kcal·mol^{-1} estimated for the 2-fluoro-4-(1-azetidinyl)benzonitrile and 3-fluoro-4-(1-azetidinyl)-benzonitrile monofluorinated derivatives in cyclopentante.[12]

As a consequence of the fact that the non radiative decay from S_1 to the ground state is almost a barrierless process in ABN-4F, internal conversion becomes the dominant process in this system, in contrast with the results obtained for ABN, where the lowest barrier for radiationless deactivation was 8.7 kcal·mol^{-1},[6] making this channel only accessible at high temperatures. The fluorine atoms enhance the tendency of sp^3 hybridation on C atoms, facilitating the folding of the ring and lowering the energy of these paths for fluorinated derivatives.

For DMABN we found two CI minimum energy points, one of CT/S_0 character and the other of LE/S_0 character. For DMABN-4F, we only found one, of LE/S_0 character. Like in ABN and ABN-4F, these geometries show a strong pyramidalization of a C atom (Figure S10 of ESI†). The LE/S_0 crossing of DMABN is analogous to the CI-2 of ABN-4F, where C_2 is puckering. Its energy is 17.6 kcal·mol^{-1} higher than the LE minimum (at CASSCF level). No transition state was located in the path from this minimum to this CI, so it can be assumed that, like in the case of ABN-4F, the maximum energy point of this path is the CI itself. The CT/S_0 CI of DMABN is also analogous to the CI-4 of ABN-4F, and located 2.8 kcal·mol^{-1} above the S_1-LE minimum (at CASSCF level). The transition state of this path is 19.9 kcal·mol^{-1} high (19.8 kcal·mol^{-1} from the TICT minimum).

The LE/S_0 CI found for DMABN-4F is analogous to the CI-1 of ABN-4F, and located 3.9 kcal·mol^{-1} below the LE minimum. The transition state of the path from this minimum to the CI is only 2.6 kcal·mol^{-1} at CASSCF level.

CASPT2 results, shown in Table 4, follow the same trends, although with numerical discrepancies due to the lack of optimization of the critical geometries at this level and the differential effect of the dynamic correlation on the states involved in these critical points.

Table 4. Energies relative to the LE minimum (in kcal·mol^{-1}) of the conical intersections and transition states involved in the radiationless deactivation of DMABN and DMABN-4F. CASSCF energies averaged for S_1 and S_0 at the CI.

DMABN					
Structure	E_{CASSCF}	$E_{CASPT2}[S_1,S_0]$	Structure	E_{CASSCF}	E_{CASPT2}
CI LE/S_0	17.6	[27.3,37.5]			
CI CT/S_0	2.8	[-2.4,-13.5]	TS	19.9	8.2
DMABN-4F					
CI LE/S_0	-3.9	[-13.5,-18.8]	TS	2.6	-7.0

Globally, the nonradiative decay from S_1 to the ground state is almost a barrierless process in DMABN-4F while for DMABN the barrier is non negligible. It is noticeable that, in spite of the inaccuracies of the CASPT2 calculations, the activation barrier obtained at this level for DMABN (8.2 kcal·mol^{-1}) is in very good agreement with the 8.3 kcal·mol^{-1} estimated experimentally in n-hexane.[15] In view of these results, it can be concluded that internal conversion becomes the dominant process from the S_1-LE minimum in DMABN-4F in such a way that, if this minimum is reached, it will be quickly depopulated through the S_0/S_1-CI precluding the normal fluorescence emission. These results explain the fact that normal fluorescence could not be detected for DMABN-4F and its ICT fluorescence quantum yield in n-hexane is only $\Phi_f = 2.610^{-3}$.[13] On the other hand, the activation barrier found in DMABN explains that internal conversion in this molecule only becomes an important decay channel above room temperature.

Radiative deexcitation: Fluorescent patterns.

The eventual emission of fluorescence depends on thermodynamic and kinetic factors: we have to take into account the relative stability of the possible emitting excited species, the probability of emission from the corresponding minima (given by the oscillator strength at those minima) and the probability of other competitive deactivation channels that could allow a nonradiative return to the ground state. We will analyse here these factors altogether to explain the fluorescence patterns observed in the systems studied.

ABN. In this system the LE species is more stable than the TICT one by more than 10 kcal·mol^{-1}, and the LE oscillator strength is larger than that of the TICT state. The barrier for radiationless deactivation is high enough (around 8 kcal·mol^{-1}) to make the internal conversion not accessible at moderate temperatures. Consequently, our results explain why the most probable deactivation channel is the emission from the LE minimum, in agreement with the experimental spectrum, which shows only the normal fluorescence band. The computed vertical emission energy of 93.7 kcal·mol^{-1},[6] is also in good agreement with the 90.0 kcal·mol^{-1} measured experimentally in hexane.[13]

ABN-4F. In this case, the LE minimum is only slightly more stable that the TICT species. Since after the initial excitation the wave packet goes through the ICT/LE conical intersection and can relax along both states, both the LE and the TICT minima can be populated, but the thermodynamic equilibrium will favour the LE species. In ABN-4F, though, the oscillator strength for deactivation to the ground state is larger for the ICT state in the TICT minimum (0.007) than for the LE state in the LE minimum (0.003). On top of this, the radiationless deactivation path is very accessible from the LE structure, so this minimum will be depopulated very fast through the nonradiative channel. For this reason, although the population of the TICT minimum is less favoured by thermodynamic factors, our results predict that only ICT emission could be observed in ABN-4F in gas phase, but with a low quantum yield (only 6·10^{-5}). The agreement with the experimental observations is not only qualitative: the computed emission energy, of 75.1 kcal·mol^{-1} (obtained at CASPT2/cc-pVDZ level) agrees satisfactorily with the 71.3 kcal·mol^{-1} measured experimentally in n-hexane.[15]

All this results are collected schematically in Figure 6.

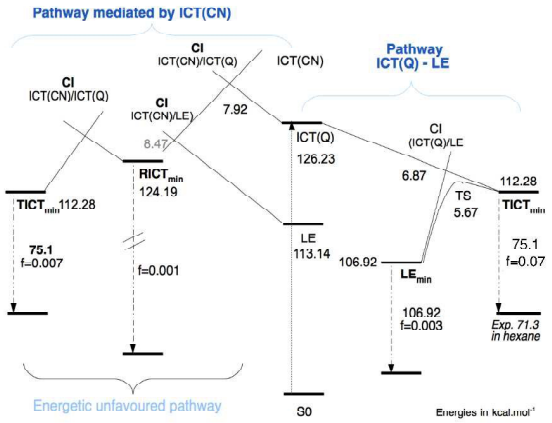

Fig. 6 Schematic representation of the most important critical points involved in the photochemistry of ABN-4F. Relative energies (in kcal·mol^{-1}) not in scale

DMABN. In this case the TICT and LE species are practically

isoenergetic due to a double effect of the alquil substituents of the amino group: first, they stabilise the ICT state due to its donor ability and second, they destabilise planar structures relative to twisted ones by steric effects. Given that the conical intersection between both states runs along the twisting coordinate and that the barrier of the adiabatic path connecting both species is low, both minima can be populated. But the probability of emission at the LE minimum is 14 times larger than at the TICT minimum, so in these circumstances the normal band is predicted to be more intense. Only when environmental factors like a polar solvent stabilise the TICT species, the anomalous emission band will be observed. If fact, experimentally, in gas phase or non polar solvent, only the LE emission is observed, while a polar environment induces the appearance of the ICT band. Similar balance of opposite factor was found to determine the fluorescence patters of aminopyrimidine derivatives.[30] The fluorescence quantum yield is high in this system at room temperature, given that the accessibility to the radiationless deactivation channel through the S_1/S_0 CI is limited by a barrier of non-negligible energy.

DMABN-4F. The characteristics of the conical intersection between the LE and TICT are the same as those reported for DMABN: there is an extended seam that runs parallel to the $CN(Me)_2$ torsion coordinate. In this case, though, the S_1-LE → S_1-TICT is an exoergic process by 17.12 kcal·mol^{-1}, in contrast to DMABN. Opposite to the other systems studied, for DMABN-4F the ICT state is the lowest energy excited state at FC. The initial excitation populates this state that relaxes without activation barrier to the TICT minimum in an ultrafast process that can end up with emission from this minimum giving place to an anomalous fluorescence band. The computed energy of this emission, 58.4 kcal·mol^{-1}, agrees satisfactorily with the 59.6 kcal·mol^{-1} obtained in n-hexane.[13] Given that the LE surface is almost degenerate with the ICT one along the relaxation path, the LE minimum can be reached, but the accessible barrierless nonradiative deactivation path will depopulate this minimum, precluding the normal emission, and decreasing the fluorescence quantum yield of this compound. These results are schematically represented in Figure 7.

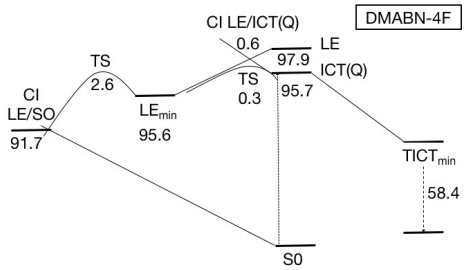

Fig. 7 Schematic representation of the most important critical points involved in the photochemistry of DMABN-4F. Relative energies (in kcal·mol^{-1}) not in scale

Conclusions

Globally, our results show that to understand the luminescence of the ABN derivatives, not only energetic factors should be considered. The competition between different possible deactivation channels has to be also taken into account. From the point of view that offers the potential energy surfaces, we can analyze the competition between radiative and radiationless deactivations with:

- the oscillator strength of the transition between the excited and the ground state at the geometry of the potential luminescent species
- the barrier of the path to the conical intersection between excited and ground state that opens the internal conversion channel.

Energetics and dynamics are affected by

a) donor ability of methyl substituents

b) electron acceptor character of fluoro substituents,

c) steric effects produced by the methyl substitution that destabilizes planar geometries and

d) enhancement by fluoro substitution of sp^2 hybridation of carbon atoms.

a) and b) favour the stabilization of the ICT state relative to the LE one; c) favours twisted species and d) stabilizes the geometries with the phenyl ring bent, what facilitates the radiationless deactivation, mainly from the LE state. The addition of these effects produces that the anomalous fluorescence band, non-existent in ABN, appears in polar solvents in the DMABN spectrum and is eventually the only band shown in the DMABN-4F spectrum. Moreover, in DMABN-4F, the steric repulsion precludes the existence of planar low-energy structures, so the GS and LE minima are pretwisted, which supports the hypothesis of a TICT structure for the CT fluorescent species.

Our study explains satisfactorily the nature of the fluorescence bands and the trends in quantum yields observed for the systems analysed. The quantitative data of absorption and emission energies computed agree satisfactorily with the experimental measurements obtained in gas phase or non-polar solvents.

As a whole, the fluorescence pattern of each of these systems depends on the contribution of several electronic and architectural factors. Small modifications in the structure of a system can lead to drastic changes in the preponderance between competitive channels. For this reason, to predict the luminescence of a system, even if the differences with other known systems are small, a detailed computational study must be performed.

Acknowledgements

Financial support has been provided by the Spanish Administration (CTQ2011-23140 and CTQ2014-51938), the Generalitat de Catalunya (2014SGR199 and Xarxa d'R+D+I en Química Teòrica i Computacional, XRQTC)

Notes and references

[a] *Departament de Química Física i Inorgànica,Universitat Rovira i Virgili. C. Marcel·lí Domingo, 1. 43007-Tarragona (Spain); E-mail: mar.reguero@urv.cat*

† Electronic Supplementary Information (ESI) available: Orbitals of the Active Space; VB-structures of DMABN-4F; geometries of the critical poins of the lowest energy PES of ABN-4F and DMABN-4F; profiles of the lowest energy PES of ABN-4F and DMABN-4F along LIIC paths joinning critical points. See DOI: 10.1039/b000000x/

1 W. Schuddeboom, S. A. Jonker, J. M. Warman, U. Leinhos, W. Kühnle, and K. A. Zachariasse, *J. Phys. Chem.*,1992, **96**,10809; U. Leinhos, *Chem. Inform.*, 1991, **95**, 2013.

2 E. Lippert, W. W. Lüder, F. Moll, W. Nägele, H. Boos, H. Prigge and I. Seybold-Blankestein, *Angew. Chem.*, 1961, **73**, 695.; Z. R. Grabowski, K. Rotkiewicz, A. Siemiarczuk, D. J. Cowley and W. Baumann, *Nouv. J. Chim*.1979, **3**, 443.

3 Z. R. Grabowski, K. Rotkiewicz and W. Rettig, *Chem. Rev.*, 2003, **103**, 3899;

4 I. Gómez, M. Reguero, M. Boggio-Pasqua and M. A. Robb, *J. Am. Chem. Soc.*, 2005, **127**, 7119.

5 J.-K. Lee, T. Fujiwara, W. G. Kofron, M. Z. Zgierski and E. C. Lim, *J. Chem. Phys.*, 2008, **128**, 164512; R. Ramos, T. Fujiwara, M. Z. Zgierski and E. C. Lim, *J. Phys. Chem. A*, 2005, **109**, 7121.

6 Mireia Segado, Isabel Gómez, and Mar Reguero, *Phys. Chem.Chem. Phys.*, 2016 (in press).

7 S. I. Druzhinin, N. P. Ernsting, S. A. Kovalenko, L. P. Lustres, T. A. Senyushkina and K. A. Zachariasse, *J. Phys. Chem. A*, 2006, **110**, 2955.

8 I. Gómez, Y. Mercier and M. Reguero, *J. Phys. Chem. A*, 2006, **110**, 11455.

9 K. A. Zachariasse, S. I. Druzhinin, V. A. Galievsky, S. Kovalenko, T. A. Senyushkina, P. Mayer, M. Noltemeyer, M. Boggio-Pasqua and M. A. Robb, *J. Phys. Chem. A*, 2009, **113**, 2693.

10 R. O. Loutfy, Can. J. Chem, 1976, 54, 1454.

11 J. N. Muller, "The theory of the Electronic Spectra of Organic Molecules", Ed. Methuen, London, 1963.

12 S. I. Druzhinin, Y. Jiang, A. Demeter and K. A. Zachariasse, *Phys. Chem. Chem. Phys.*, 2001, **3**, 5213.

13 V. A. Galievsky, S. I. Druzhinin, A. Demeter, Y. Jiang, S. A. Kovalenko, L. P. Lustres, K. Venugopal, N. P. Ernsting, X. Allonas, M. Noltemeyer, R. Machinek and K. A. Zachariasse, *Chem. Phys. Chem.*, 2005, **6**, 2307.

14 S. Murali, V. Kharlanov, W. Rettig, A. I. Tolmachev and A. V. Kropachev, *J. Phys. Chem. A*, 2005, **109**, 6420.

15 S. I. Druzhinin, A. Demeter, V. A. Galievsky, T. Yoshihara and K. A. Zachariasse, *J. Phys. Chem. A*, 2003, **107**, 8075.

16 W. J. Herhe, R. Ditchfield, R. and J. A. Pople, *J. Chem. Phys.*, 1972, **56**, 2257.

17 P. A. Malmqvist, B. O. Roos, B. O. and B. Schimmelpfennig, *Chem. Phys. Lett.*, 2002, **357**, 230.

18 L. Blancafort, P. Celani, M. J. Bearpark and M. A. Robb, *Theor. Chem. Acc. Theor. Comput. Model. Theor. Chim. Acta*, 2003, **110**, 92–99.

19 Gaussian 09, Revision A.02, M. J. Frisch, G. W. Trucks, H. B. Schlegel, G. E. Scuseria, M. A. Robb, J. R. Cheeseman, G. Scalmani, V. Barone, B. Mennucci, G. A. Petersson et al., Gaussian, Inc., Wallingford CT, 2009.

20 F. Aquilante, L. Vico, N. Ferré, G. Ghigo, P. A. Malmqvist, P. Neogrády, T. B. Pedersen, M. Pitoňák, M. Reiher, B. O. Roos et al. *J. Comp. Chem.*2010, **31**, 224.

21 O. Kajimoto, H. Yokoyama, Y. Ooshima and Y. Endo, *Chem. Phys. Lett.*1991, **179**, 455.

22 A. Heine, R. Herbst-Irmer, D. Stalke, W. Kühnle and K. A. Zachariasse, *Acta Crystallogr*., 1994, **B50**, 363.

23 R. Nakagaki, S. Kohtani and Y. Nakamura, *Anal. Sci.* 2003, **19**, x5

24 S. Murali, V. Kharlanov, W. Rettig, W., A. I. Tolmachev and A. V. Kropachev, *J. Phys. Chem A,* 2005, **109**, 6420.

25 V. A. Galievsky, S. I. Druzhinin, A. Demeter, Y. Jiang, S. A. Kovalenko, L. P. Lustres, K. Venugopal, N. P. Ernsting, X. Allonas, M. Noltemeyer, R. Machinek, and K. A. Zachariasse. *Chem. Phys. Chem.*, 2005, **6**, 2307.

26 W. Schuddeboom, S. A. Jonker, J. H. Warman, U. Leinhos, W. Künhle and K. A. Zachariase, *J. Phys. Chem.*, 1992, **96**, 10809.

27 P. B. Coto, L. Serrano-Andreés, T. Gustavsson, T. Fujiwara and E. C. Lim, *Phys. Chem. Chem. Phys.*, 2011, **13**, 15182.

28 I. Gómez, P. J. Castro and M. Reguero, *J. Phys. Chem. A*, 2015, **119**, 1983.

29 A. Perveaux, P. J. Castro, D. Lauvergnat, M. Reguero and B. Lasorne, *J. Phys. Chem. Lett.*, 2015, **6**, 1316.

30 M. Segado, M. A. Carvajal, I. Gómez, M. Reguero, *Theor. Chem. Acc.*, 2011, **128**, 713.